Ground state and low energy spectrum of kagome antiferrmagnet YCu_3-Br/Cl

Chengkang Zhou[1], Zhenyuan Zeng[2], Bin-Bin Chen[1], Zi Yang Meng[1], Shiliang Li[2]
1 Department of Physics, The University of Hong Kong
2 Institute of Physics, Chinese Academy of Sciences

Scan and Download

Material

We studied the magnetic properties of $YCu_3(OH)_6Br_2[Br_{(1-x)}(OH)_x]$ (YCu_3-Br) where Cu^{2+} ions form **2D kagome** layers ①②③. In this material, we observed a **non-magnetic order ground state** down to 50 mK, while the Curie-Weiss temperature is around -100 K. At zero magnetic field, the specific heat at low temperatures follows a **T^2 dependence**. Furthermore, the spin excitation spectrum is consistent with the prediction from the Dirac spinon. All of these findings suggest that the material may hold a ground state of a **Dirac quantum-spin-liquid (QSL) state**.

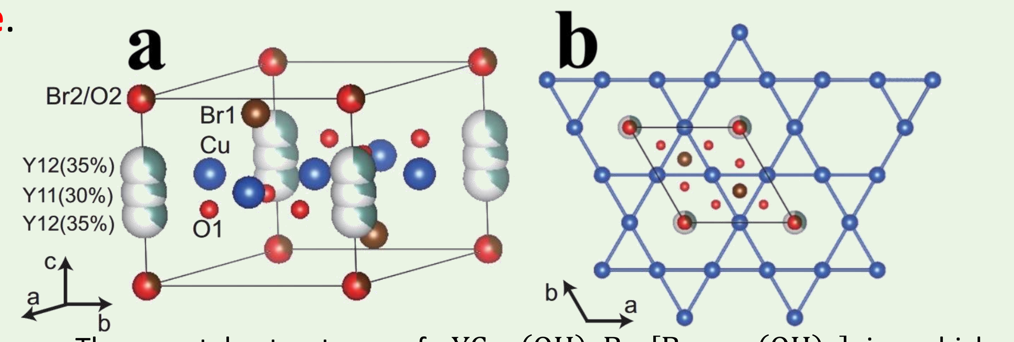

FIG.1. **a**, The crystal structure of $YCu_3(OH)_6Br_2[Br_{(1-x)}(OH)_x]$ in which hydrogens are not shown. The solid lines represent the unit cell. **b**, The Kagome plane of Cu 2+ ions viewed along the c axis. The other atoms are shown in only one unit cell.

Magnetic Susceptibility & Specific Heat

The magnetic susceptibility and specific heat are plotted here. Fig.2(a) displays the $\chi^{-1} = H/M$ of YCu_3-Br as a function of T. A linear fit to the data above 150 K provides the Curie-Weiss temperature θ_{CW} and the effective moment μ_{eff}, estimated to be about -79 K and $1.94\mu_B$, which suggests significant AFM interactions but no long-range magnetic order ①③⑤⑥.

Meanwhile, Fig.2(b-d) illustrate the C/T behavior as follows:

$$\frac{C}{T} = \frac{A}{T^3} + \alpha T^n \ (n = 1 \pm 0.02, H = 0T),$$

$$\frac{C}{T} = \gamma + \alpha T \ (H > 0T),$$

with $\gamma \propto B$ (see Fig.2d).

These findings (**$C \propto T^2$** and **$\gamma \propto B$**) indicate that the ground state is a candidate for a Dirac QSL state ⑦.

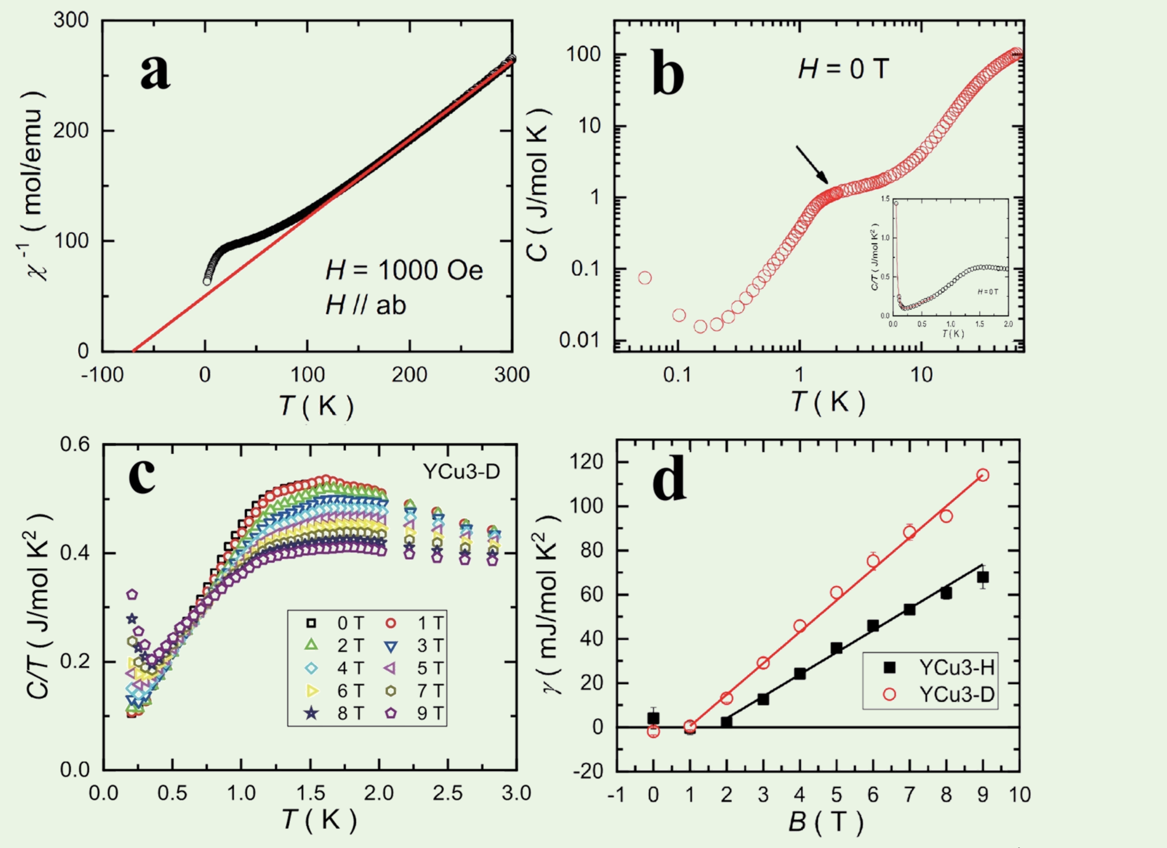

FIG.2 **a**, The temperature dependence of the inverse of the magnetic susceptibility χ^{-1}. The solid line is a linear fit for the high-temperature data. **b**, The temperature dependence of the specific heat C in the log-log scale. The inset shows C/T below 2 K at 0 T. **c**, The temperature dependence of C/T at different fields for YCu3-D. **d**, The field dependence of γ. The solid lines are fitted results with the linear function.

Spectra Evidence

To further identify the ground state of YCu_3-Br, inelastic neutron scattering (INS) is applied to investigate its low-energy spin excitation. Although it is difficult to directly detect single **Dirac spinon excitations**, which are the crucial features of a Dirac QSL state, two spinon excitations with a total spin quantum number S=1 can result in a spin continuum that can be revealed by INS, as illustrated in Fig. 3. Fig. 4 displays our INS results. The key finding in our work is the low-energy **conical spin excitations with a continuum inside**, which requires a non-trivial origin for the low-energy excitations and can be well explained by the presence of Dirac spinons. This results in conical spin excitations due to two-spinon convolution.

To explain this observation, the distorted Kagome model is considered, with its Hamiltonian (see Fig.5 a):

$$H = J_1 \sum_{\langle i,j \rangle_1} S_i\ S_j + J_2 \sum_{\langle i,j \rangle_2} S_i\ S_j + J_h \sum_{\langle i,j \rangle_h} S_i\ S_j \quad ❶$$

Additionally, the linear spin wave (LSW) is applied based on this model in the Q = (1/3, 1/3) (see Fig.5 b) ordered phase ④ (see Fig. 5 c-h).

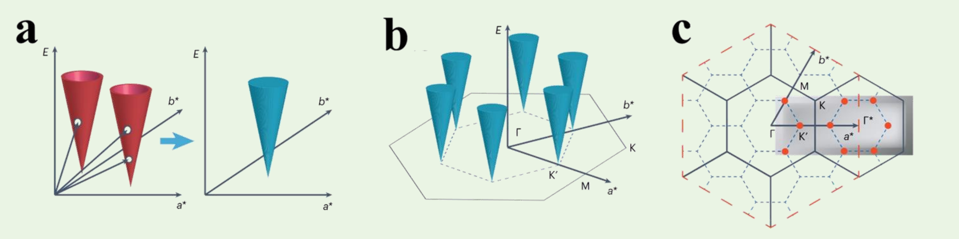

FIG. 3 Schematics of low-energy conical spin excitations and reciprocal space for YCu_3-Br. **a**, Schematic illustration of two Dirac spinons with a conical surface dispersion (red) that merge into a cone spin excitation with a continuum inside (blue). **b**, Six conical low-energy spin excitations in YCu_3-Br. Their momenta in the kagome Brillouin zone is indicated. **c**, Sketch of the in-plane reciprocal space. The black solid line and the red and blue dashed lines represent the kagome, the extended kagome and the lattice of the distorted Kagome model ❶ Brillouin zones, respectively. The grey shaded area illustrates the regime measured in this experiment.

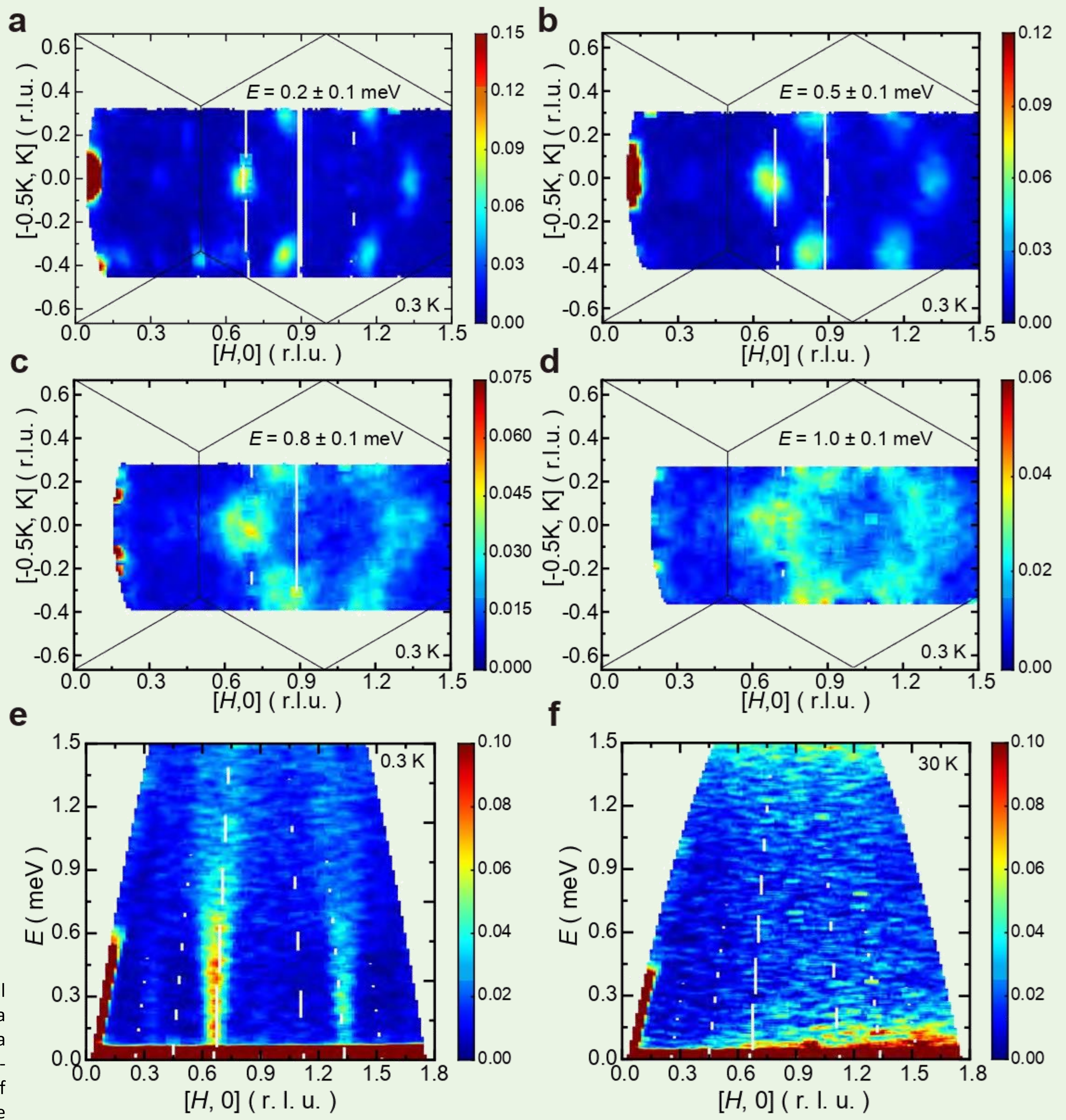

FIG.4 Spin excitations in $YCu_3(OD)_6Br_2[Br_{0.33}(OD)_{0.67}]$ measured via the neutron scattering. **a-d**, Intensity contour plots of the INS results at 0.3 K in the [H,K] zone at 0.2, 0.5, 0.8 and 1 meV, respectively. **e,f**, Intensity contour plots of the INS results as a function of E and Q along the [H, 0] direction at 0.3 K (e) and 30 K (f).

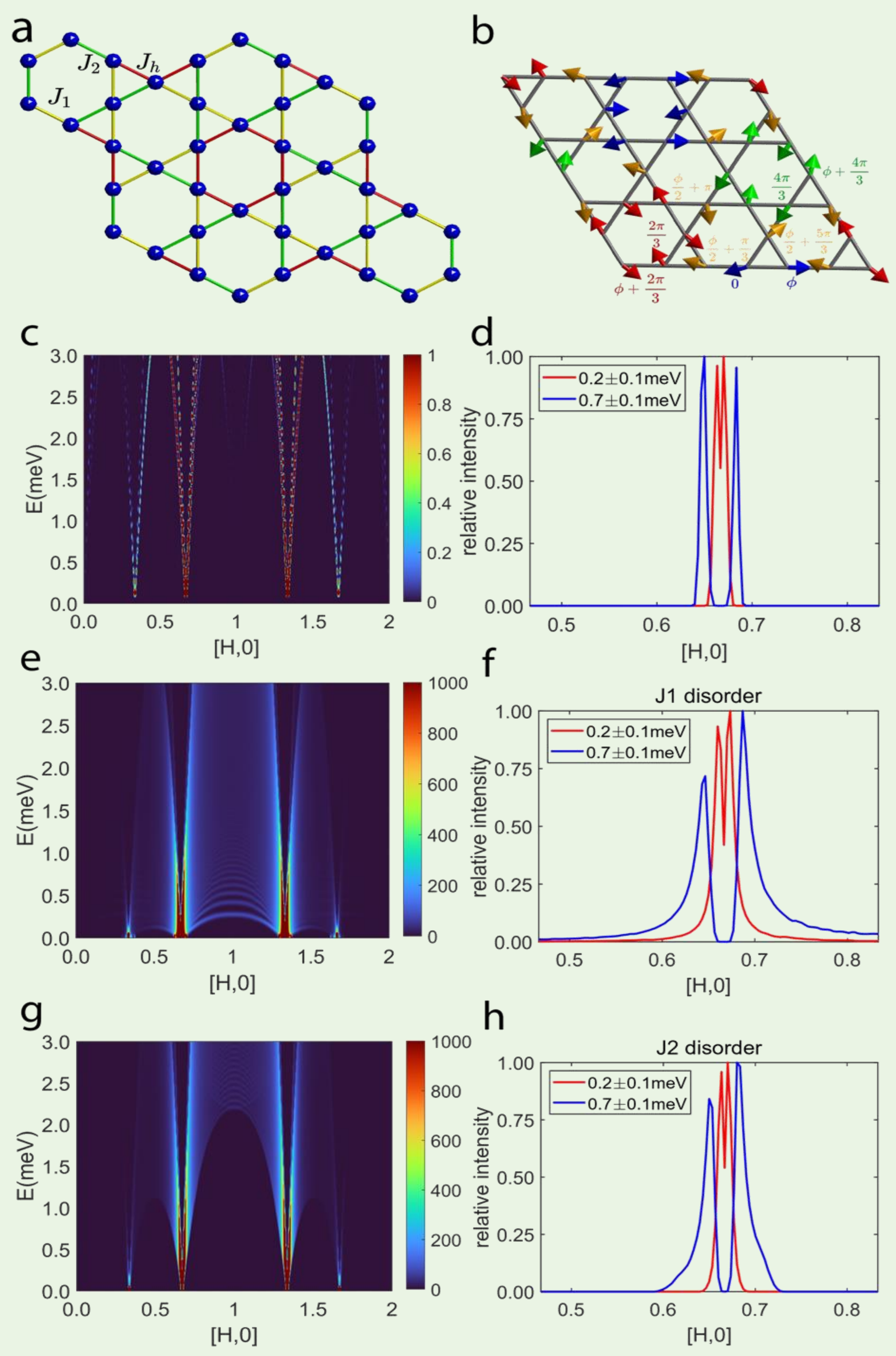

FIG.5 **a** and **b** depict the distorted Kagome model ❶ and the Q=(1/3, 1/3) order, respectively. **c** and **d** present the LSW spectra without introducing disorder effects. **e-h** display the spectra with the same parameters but with introduced disorder effects. In this case, we chose $(J_1, J_2, J_h) = (39.3meV, 20.3meV, 39.3meV)$ to enable the upper limit of the spectra to reach E ≈ 7.5meV, consistent with experimental observations. **e-f** show the spectral functions with a 20% distribution on the J_1 bond, which ranges from 31.4meV to 39.4meV. Likewise, **g-h** present the spectral functions with a 20% distribution on the J_2 bond, ranging from 16.3meV to 20.3meV.

DMRG simulations

Via density matrix renormalization group (DMRG) calculations, we investigate the distorted Kagome model ❶ as it starting from the Q=(1/3, 1/3) ordered phase (the red region in the phase diagram from ④) towards the isotropic Kagome Heisenberg limit in two different path (the green arrow). Our results are plotted in Fig. 6. It is worth noting that our results also show consistency with experimental findings, such as the DMRG intensity along the cyan line in Fig. 6**e** (shown as the cyan line in **q**), which corresponds with the blue line in **q**.

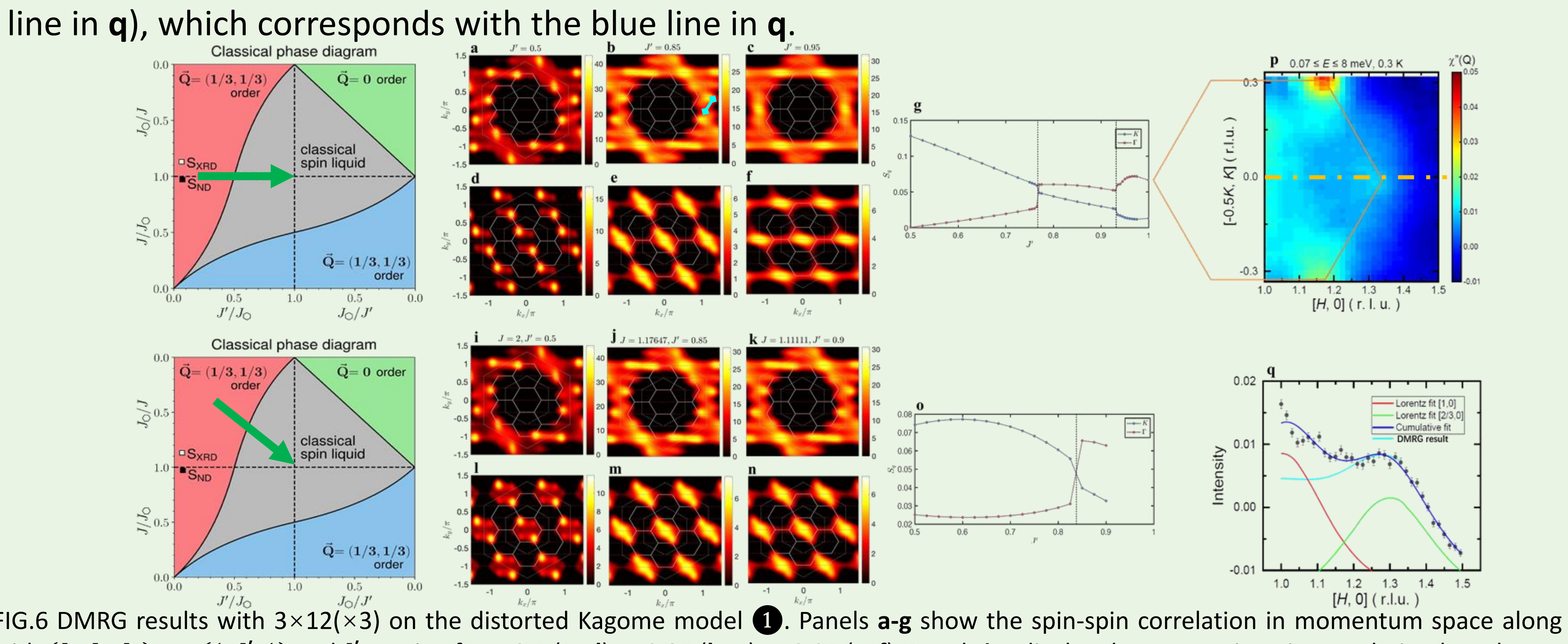

FIG.6 DMRG results with 3×12(×3) on the distorted Kagome model ❶. Panels **a-g** show the spin-spin correlation in momentum space along with $(J_1, J_2, J_h) = (1, J', 1)$ and J' ranging from 0.5 (**a, d**) to 0.85 (**b, e**) to 0.95 (**c, f**). Panels **i-o** display the same spin-spin correlation but along a different path with $(J_1, J_2, J_h) = (1/u, u, 1)$ and u ranging from 0.5 (**i, l**) to 0.85 (**j, m**) to 0.9 (**k, n**). Panels **a-c** and **i-k** illustrate the $S_q = \sum_{i,j} \langle S_i S_j \rangle e^{iq \cdot R_{ij}}$ while panels **d-f** and **l-n** shows $S_q^A = \sum_{i,j \in A} \langle S_i S_j \rangle e^{iq \cdot R_{ij}}$ for the same sublattice. In panels **g** and **o**, the blue line represents the correlation function for the same sublattice at the K point, while the red one is for the Γ point. The phase diagram is adapted from ④**.** In **p**, the correlation is obtained by integrating the spectrum in INS from 0.07 meV to 8 meV at 0.3 K, and the orange line refers to the Brillouin zones of the distorted Kagome model. **q** represents a line-cut of **p** that crosses the Dirac point along the orange dashed line. The cyan line is for the DMRG result along the cyan line in **b**. The intensity of the DMRG result has been rescaled to align the peak at 1.3 with the experimental results.

Bond Randomness

The magnetic properties of $YCu_3(OH)_6[(Cl_xBr_{1-x})_{3-y}(OH)_y]$($YCu_3$-Br/Cl) have also been investigated, where there are two types of hexagons: uniform hexagons (UHs, shown on the left in Fig. 7a) and alternate-bond hexagons (ABHs, shown on the right in Fig. 7a), denoted as s and n, respectively. These differences arise from the varying Cu-O-Cu angles, and it should be noted that YCu_3-Cl has a negligible percentage of ABHs, while YCu_3-Br has a significantly higher count. We can observe that the AFM order emerges when $n/(n+s) \lesssim 1/3$, while the possible QSL state arises when **$n/(n+s) \gtrsim 2/3$**.

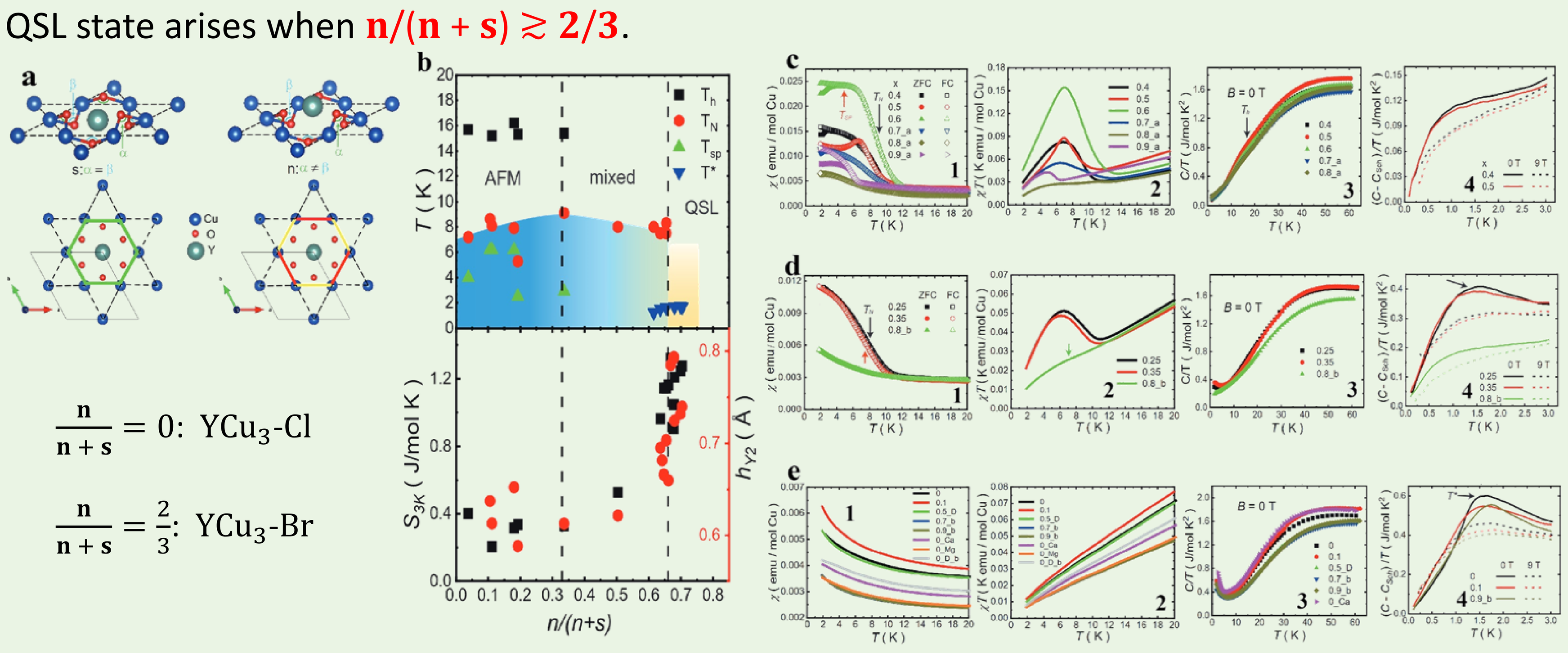

$$\frac{n}{n+s} = 0: \ YCu_3\text{-Cl}$$

$$\frac{n}{n+s} = \frac{2}{3}: \ YCu_3\text{-Br}$$

FIG.7 **a** The schematic diagram of the local crystal structure consists of uniform hexagons (UHs) on the left and alternate-bond hexagons (ABHs) on the right, denoted as s and n, respectively. **b** The magnetic phase diagram of the YCu_3-Br/Cl system. And the corresponding entropy below 3 K (black point) and the height of out-of-plane yttrium h_{Y2}(red point), with the value of n/(n + s) as the variable. **c, d, and e**: The magnetic susceptibility (1-2) and specific heat (3-4) of the antiferromagnetic (AFM) ordered, mixed, and possible quantum-spin-liquid (QSL) samples, respectively.

Bibliography

①,arXiv:2311.13089, Aini Xu, Shiliang Li, et al; ②,Nat. Phys. (2024), Zhenyuan Zeng, et al; ③,Phys. Rev. B 105, L121109 (2022),Zhenyuan Zeng, et al; ④,npj Comput Mater 8, 10 (2022), Hering, M., et al; ⑤, Phys. Rev. B 105, 024418(2022) ,Jiabin Liu, et al; ⑥, J. Magn. Magn. Mater. 512, 167066 (2020) X.-H. Chen et al; ⑦, Phys. Rev. Lett. 98, 117205 (2007) Ying Ran., et al.